

1 **Title: Controls on millennial-scale atmospheric CO₂ variability during the last glacial period**

2

3 Authors:

4 Bauska, T.K.^{1,2*}, Brook, E.J.², Marcott, S.A.³, Baggenstos, D.⁴, Shackleton, S.⁴, Severinghaus, J.P.⁴,

5 Petrenko, V.V.⁵

6

7 1: Godwin Laboratory for Palaeoclimate Research, Department of Earth Sciences, University of

8 Cambridge, Downing Street, CB2 3EQ, United Kingdom

9

10 2: College of Earth, Ocean, and Atmospheric Sciences, Oregon State University, 104 CEOAS Admin Bldg,

11 Corvallis, OR 97331, USA

12

13 3: Department of Geoscience, University of Wisconsin-Madison, 1215 W Dayton St. Madison, WI

14 53706, USA

15

16 4: Scripps Institution of Oceanography (SIO), University of California, San Diego, La Jolla, CA, 92093,

17 USA.

18

19 5: Department of Earth and Environmental Sciences, University of Rochester, Rochester, NY 14627,

20 USA

21

22 *tkb28@cam.ac.uk

23

24 **Key points**

25

26 • A new ice core record of the stable isotopes of atmospheric CO₂ suggests organic carbon

27 sources controlled CO₂ levels during the last glacial period

28

29 • The millennial-scale CO₂ variability is tentatively linked to variations in Southern Ocean carbon

30 sources

31

32 • Centennial-scale CO₂ variability during the last glacial period is associated with similarly

33 abrupt changes during the deglaciation

34

35

36 **Abstract**

37 Changes in atmospheric CO₂ on millennial-to-centennial timescales are key components of past
38 climate variability during the last glacial and deglacial periods (70-10ka) yet the sources and
39 mechanisms responsible for the CO₂ fluctuations remain largely obscure. Here we report the ¹³C/¹²C
40 ratio of atmospheric CO₂ during a key interval of the last glacial period at sub-millennial resolution,
41 with coeval histories of atmospheric CO₂, CH₄ and N₂O concentrations. The carbon isotope data
42 suggest that the millennial-scale CO₂ variability in MIS3 is driven largely by changes in the organic
43 carbon cycle, most likely by sequestration of respired carbon in the deep ocean. Centennial-scale CO₂
44 variations, distinguished by carbon isotope signatures, are associated with both abrupt hydrological
45 change in the tropics (e.g. Heinrich Events) and rapid increases in northern hemisphere temperature
46 (DO events). These events can be linked to modes of variability during the last deglaciation, thus
47 suggesting that drivers of millennial and centennial CO₂ variability during both periods are intimately
48 linked to abrupt climate variability.

49

50 **Plain Language Summary**

51 Ice cores provide unique records of variations in atmospheric CO₂ prior to the instrumental era. While
52 it is clear that changes in atmospheric CO₂ played a significant role in driving past climate change, it is
53 unclear what in turn drove changes in atmospheric CO₂. Here we investigate enigmatic changes in
54 atmospheric CO₂ levels during an interval of the last glacial period (~50,000 to 35,000 years ago) that
55 are associated with abrupt changes in polar climate. To determine the sources and sinks for
56 atmospheric CO₂ we measured the stable isotopes of carbon in CO₂ and found that the primary source
57 of carbon to the atmosphere was an organic carbon reservoir. Most likely, this carbon was sourced
58 from a deep ocean reservoir that waxed and waned following changes in either the productivity of the
59 surface ocean or stratification of the deep ocean. We also found that atmospheric CO₂ can change on
60 the centennial time-scale during abrupt climate transitions in the Northern Hemisphere. This
61 observation adds to a growing body of evidence that abrupt changes in atmospheric CO₂ are an
62 important component of past carbon cycle variability.

63

64

65

66

67

68

69

70

71

72

73 **Introduction**

74 In order to predict the climate impacts of anthropogenic CO₂ emissions over the coming millennia
75 (Clark et al., 2016) we must understand how the climate system and carbon cycle have interacted over
76 these same timescales in the past. The CO₂ rise during the last deglaciation, arguably the most well-
77 studied example of past carbon cycle variability, is likely a combination of millennial-scale climate
78 change and glacial-interglacial shifts in temperature and ice volume, which are all amplified through a
79 system of climate-carbon cycle feedbacks. To disentangle the millennial-scale component we
80 investigate carbon cycle variability of the last glacial period when climate variations were largely
81 unaffected by changes in northern hemisphere insolation and ice volume that characterize glacial
82 terminations (Figure S1).

83

84 During Marine Isotope Stage 3 (MIS3) atmospheric CO₂ varied between about 195 and 225 ppm with a
85 roughly triangular waveform (Indermühle, 2000) (Figure 1 E). This pattern mimics Antarctic
86 temperature, rising during the strongest Antarctic warmings and falling during the coolings (Figure 1
87 B). From the perspective of Greenland climate and the well-known Dansgaard-Oeschger events (DO),
88 CO₂ increases during cold phases (stadials)(Ahn & Brook, 2008) with the most prominent increases
89 corresponding to only those stadials associated with an enhanced flux of debris-laden ice to the North
90 Atlantic (known as a Heinrich Events; these specific cold intervals are often referred to as “Heinrich
91 stadials”). CO₂ decreases after a rapid switch to warmer conditions over Greenland (interstadials) and
92 slower cooling in Antarctica (Bereiter et al., 2012). This strong relationship between Antarctic
93 temperature and CO₂ has focused attention on the Southern Ocean (SO) as the major conduit for the
94 transfer of carbon between the atmosphere and the ocean on millennial and glacial-interglacial
95 timescales (Sigman et al., 2010), with possible triggers in the North Atlantic.

96

97 The ratios of carbon isotopes differ among key carbon reservoirs and thus some of the sources and
98 sinks driving past atmospheric CO₂ can be constrained using the isotopic composition of atmospheric
99 CO₂ (Bauska et al., 2016; Schmitt et al., 2012; Köhler et al., 2006; Eggleston et al., 2016). Four major
100 processes fractionate the carbon isotopes ($\epsilon_{A-B} \sim \delta^{13}C_A - \delta^{13}C_B$): photosynthesis that makes CO₂ into
101 organic carbon on land ($\epsilon_{\text{land-atmosphere}} = \sim -18\text{‰}$), photosynthesis in the surface ocean that forms
102 particulate organic carbon from dissolved inorganic carbon ($\epsilon_{\text{DIC-POC}} = \sim -22\text{‰}$), air-sea gas exchange
103 ($\epsilon_{\text{DIC-atmosphere}} = +\sim 8\text{‰}$; decreasing by 0.1‰ for every 1°C increase in ocean temperature), and a
104 negligible fractionation during the formation of CaCO₃ in surface ocean, ($\epsilon_{\text{DIC-CaCO}_3} = \sim 0\text{‰}$). By
105 measuring the time varying changes in both atmospheric CO₂ concentrations and the $\delta^{13}C$ isotopes, we
106 can constrain the sources of the CO₂ changes. Rising atmospheric CO₂ and decreasing $\delta^{13}C$ -CO₂ is
107 consistent with organic carbon sources to the atmosphere; rising atmospheric CO₂ and increasing
108 $\delta^{13}C$ -CO₂ is consistent with a warming ocean; and rising CO₂ with no changes in $\delta^{13}C$ -CO₂ could indicate
109 a balanced contribution of rising ocean temperature and organic carbon sources or the influence of

110 CaCO₃ or volcanic sources. Air-sea gas exchange in the high-latitude ocean may affect atmospheric
111 $\delta^{13}\text{C-CO}_2$, with rising atmospheric CO₂ and large decreases in $\delta^{13}\text{C-CO}_2$ predicted by box model
112 experiments that include enhanced air-sea gas exchange in the SO (Bauska et al., 2016; Köhler et al.,
113 2006). Finally, changes in the abundance of C3 and C4 plants on land (Ehleringer et al., 1997) or
114 ecological shifts in marine biosphere (Broecker & McGee, 2013) would change the overall
115 photosynthetic fractionation and thus the details, but not the fundamentals, of using $\delta^{13}\text{C-CO}_2$ to
116 fingerprint carbon sources.

117
118 Other atmospheric gases provide additional constraints on carbon cycle variability, particularly
119 related to the response of the terrestrial biosphere to abrupt climate change. Most evidence suggests
120 that past variations in methane are dominated by climate variability over tropical and boreal wetlands
121 (Brook et al., 2000; Rhodes et al., 2015). N₂O is produced in oxygen-poor ocean waters and terrestrial
122 soils. Rising N₂O most likely reflects either decreasing oxygen levels in the intermediate-depth ocean,
123 warmer terrestrial soil temperatures or a combination of the two (Schilt et al., 2014). The $\delta^{18}\text{O-O}_2$
124 largely follows the changes in $\delta^{18}\text{O}$ of seawater and orbitally-driven changes in the Dole effect, but
125 rapid increases in $\delta^{18}\text{O-O}_2$ have been argued to reflect southward shifts in low-latitude precipitation
126 (Seltzer et al., 2017; Severinghaus et al., 2009) (see SI for definition of Δ_{ELAND}).

127 128 **Methods and Materials**

129 We present new atmospheric histories of CO₂, N₂O, CH₄ and $\delta^{13}\text{C-CO}_2$ spanning 47-35 ka from the
130 Taylor Glacier, Antarctica blue ice area (Figure 1 D-G). The chronology (Baggenstos et al., 2017) is
131 constructed by synchronizing the Taylor Glacier CH₄ and $\delta^{18}\text{O-O}_2$ records to the WDC timescale
132 (Buizert et al., 2015) and thus linking to the radiometrically dated Hulu Cave record (Cheng et al.,
133 2016) (Figure 1 C). The concentrations of CO₂ and N₂O and the $\delta^{13}\text{C-CO}_2$ were measured on the same
134 sample using the Oregon State University ice grater system (Bauska et al., 2014). The long-term
135 reproducibility for CO₂, N₂O and $\delta^{13}\text{C-CO}_2$ are $\pm 1\text{ppm}$, $\pm 5\text{ppb}$, $+0.02\text{‰}$, respectively (Bauska et al., 2015;
136 Bauska et al., 2016). The combination of increased resolution and precision equates to a significant
137 improvement over previous reconstructions which focused on longer-term changes (Eggleston et al.,
138 2016) (Figure S1). Additionally, previous reconstructions in this time interval were limited by offsets
139 between cores (see *Eggleston et al., 2016* for detailed discussion and Figure S2). Using the interval
140 from 47 to 43ka as a baseline for comparison, the Talos Dome $\delta^{13}\text{C-CO}_2$ record has significantly lower
141 and more variable values (mean \pm s.d. = $-6.72\pm 0.23\text{‰}$; n = 12) than data from the EDML ($-6.50\pm 0.12\text{‰}$;
142 n = 8) and EDC ($-6.59\pm 0.16\text{‰}$; n = 5) ice cores. In the same interval, the Taylor Glacier averages -
143 $6.55\pm 0.07\text{‰}$ (n = 14) in broad agreement with EDML and EDC. Although we can confidently interpret
144 relative changes in our new record because of the improvement in precision and resolution,
145 addressing the absolute accuracy of the $\delta^{13}\text{C-CO}_2$ values requires additional inter-laboratory and inter-
146 core comparison.

147

148 **Results: Ice Core Constraints on Greenhouse Gas Variability**

149 The most salient mode of variability in atmospheric CO₂, the millennial-scale rising and falling with
150 Antarctic temperature, is accompanied by an inversely correlated change in δ¹³C-CO₂ (Figure 1 E-F).
151 Atmospheric CO₂ ranges from about 195 to 215 ppm with the corresponding variability in δ¹³C-CO₂
152 spanning -6.45 to -6.65‰ (a -0.1‰ change for every +10 ppm). At finer scales we observe several
153 other modes of variability. The CO₂ rise during Heinrich Stadial 4 (40.2-38.4 ka; “HS4”) starts off
154 slowly, rising 3-4 ppm while δ¹³C-CO₂ decreases by ~0.05‰. As noted previously in the Siple Dome ice
155 core (Ahn & Brook, 2014), the rise then accelerates in a sharp jump of about 8 ppm. The rapid phase of
156 the rise is coincident with the mid-stadial rise in CH₄ noted in the WAIS Divide Core (Rhodes et al.,
157 2015) (Figure 1 D, red vertical line) and the increase in Δε_{LAND} first observed in the Siple Dome Core
158 (Severinghaus et al., 2009) and confirmed in the WDC record (Seltzer et al., 2017) (Figure 1 H). No
159 change in N₂O is resolved in the Taylor Glacier dataset, consistent with the Talos Dome record (Schilt
160 et al., 2010) (Figure 1 G). The resolution of the carbon isotope measurements prevents a clear
161 fingerprinting of the source but a replicated sample clearly falls to more negative values off the more
162 gradual trend by about 0.1‰ (Figure 1 F). In the later part of the HS4, CO₂ continues to rise slowly by
163 3 ppm and δ¹³C-CO₂ decreases by another 0.1‰.

164

165 The onsets of DO interstadials are accompanied by small rises in CO₂ (Figure 1 E, dashed gray lines).
166 This variability has been noted in other cores and described as either a lagged response to Antarctic
167 temperature (Bereiter et al., 2012) or, in the case of the weaker DO events, a lagged response to
168 Greenland stadial conditions that are too short to impart a significant change in CO₂ (Ahn & Brook,
169 2014). In our record we note that atmospheric CO₂ appears to increase along with CH₄, and N₂O with
170 no discernable lead or lag. This is most prominent at DO8 when CH₄ rises by about 120 ppb, N₂O rises
171 by 35 ppb and CO₂ rises by 6 ppm (see also Figure 4 n-p). The other DO events (7,9,10) are near the
172 detection limit of our record and difficult to quantify. Across these events δ¹³C-CO₂ either increases
173 slightly (~0.08‰ at DO8) or shows no substantial change.

174

175 **Discussion: Millennial-scale carbon cycle variability**

176 The overall negative correlation between CO₂ and δ¹³C-CO₂ rules out changes in ocean temperature,
177 the CaCO₃ cycle, or volcanic input having a dominant role in driving millennial-scale CO₂ (Figure 2).
178 Instead, the data are consistent with changes in terrestrial carbon storage or the strength of the
179 ocean’s biological pump. If terrestrial sources were dominant, whole ocean δ¹³C would follow
180 atmospheric δ¹³C-CO₂. If oceanic sources from changes in the strength of the biological pump or shifts
181 in ocean ventilation were dominant, the surface-to-deep gradient in δ¹³C in inorganic carbon in the
182 ocean would decrease along with atmospheric δ¹³C-CO₂.

183

184 Millennial-scale decreases in the vertical gradient of $\delta^{13}\text{C}$ in the SO have been tentatively correlated to
185 maxima in atmospheric CO_2 (Charles et al., 2010; Ziegler et al., 2013), and therefore in light of our new
186 data, minima in $\delta^{13}\text{C}\text{-CO}_2$ (Figure 3a-b). If this coupling of the oceanic gradient of $\delta^{13}\text{C}$ and atmospheric
187 $\delta^{13}\text{C}\text{-CO}_2$ could be demonstrated to be precisely in-phase it would provide clear evidence of an oceanic
188 source controlling atmospheric CO_2 . Taking the current data and chronology at face-value, the
189 decreases in the oceanic $\delta^{13}\text{C}$ gradient are broadly associated with minima in atmospheric $\delta^{13}\text{C}\text{-CO}_2$,
190 yet the coupling is clearly not one-to-one, possibly due to chronological errors in the marine sediment
191 record. To explore this hypothesis further, we combined existing benthic carbon isotope records from
192 deep SO ($\sim 42^\circ\text{S}$, 10°E , 4600 m) (Charles et al., 1996; Ninnemann et al., 1999; Hodell et al., 2001, 2003).
193 These records use previously established age models tied to the Greenland ice core records using
194 carbonate preservation and confirmed by ^{14}C data during the deglaciation and the Laschamp
195 paleomagnetic event during MIS3 ($\sim 42\text{ka}$) (Barker & Diz, 2014). We include a minor increase in the
196 absolute age of 0.63% to account for the possible under-counting of annual layers in the Greenland Ice
197 Core chronologies relative to the WAIS Divide timescale (Buizert et al., 2015).

198
199 We note that the atmosphere and deep ocean $\delta^{13}\text{C}$ are anti-correlated during MIS3 (Figure 3c). This
200 supports the hypothesis that the waxing and waning of respired organic carbon source in the deep SO
201 controlled atmospheric CO_2 and significantly limits the possibility of contributions from terrestrial
202 sources. However, this relationship alone cannot delineate oceanic sources between changes in export
203 productivity and changes in stratification. Evidence to support changes in export productivity comes
204 from the correlation of the ice core data and foraminifera-bound $\delta^{15}\text{N}$ which indicates lower nitrate
205 utilization during periods of high atmospheric CO_2 (Martínez-García et al., 2014) (Figure 3d). Iron
206 deposition rates and export production in the Subantarctic are also closely coupled, suggesting that
207 the extent of iron limitation may have played a role in this enhanced nutrient utilization (Jaccard et al.,
208 2016). Evidence in support of ventilation changes stems from radiocarbon constraints in the South
209 Atlantic that are closely coupled with deep ocean oxygen levels, suggesting that both export
210 productivity and ocean circulation were working in concert over this period (Gottschalk et al., 2016).
211 A quantitative description of this coupling requires study with isotope enabled earth system models;
212 however, additional insight can be gained by comparing to periods when these processes may have
213 become uncoupled.

214
215 Our new high-resolution MIS3 data now provide a similar sequence of abrupt climate change events to
216 contrast with the last deglaciation. First, we compare the MIS3 data to the last deglaciation utilizing a
217 cross plot of CO_2 and $\delta^{13}\text{C}\text{-CO}_2$ (Figure 2). We see that the MIS3 data fall along the same trend observed
218 during HS1 of the last deglaciation ($\sim 18\text{-}15.0\text{ka}$) yet only span about 50% of range (note that the low
219 $\delta^{13}\text{C}\text{-CO}_2$ values that fall off this trend are due to centennial-scale variability at $\sim 16.3\text{ka}$). This suggests
220 that millennial-scale CO_2 variations in MIS3 can be linked mechanistically to the more pronounced

221 variability during the deglaciation. As discussed in previous work, this co-variability of CO₂ and δ¹³C-
222 CO₂ is consistent with changes in SO ventilation (Köhler et al., 2006; Menviel et al., 2015; Schmitt et al.,
223 2012; Tschumi et al., 2011) changes in export production (particularly the SO)(Bauska et al., 2016;
224 Menviel et al., 2012) or a weakening of the ocean's biological pump by a reduction in North Atlantic
225 Deep-water (NADW) formation (Schmittner & Lund, 2015).

226
227 Second, we compare the two intervals in time with the GHG records plotted over 8ka intervals (Figure
228 4a-c). Similar patterns of millennial-scale variability in CH₄ and N₂O are observed but the changes in
229 CO₂ appear fundamentally different. First, the CO₂ rise during HS1 is about 20 ppm greater than the
230 rise in HS4 (or ~2x) and, second, CO₂ remains elevated after the switch to interstadial conditions
231 during the Bølling-Allerød (BA) rather than decreasing as observed after the onset of DO8 (Figure 3 C).
232 The δ¹³C-CO₂ follows a similar pattern. In HS1 δ¹³C-CO₂ decreases by 0.2‰ more than HS4 and
233 stabilizes during the BA as opposed to abrupt increases observed during DO8 (Figure 4 D). What was
234 different about the deglaciation that allowed more respired carbon into the atmosphere during HS1
235 than HS4 and prevented, or compensated for, a potential uptake of carbon during the BA?

236
237 During the Heinrich stadials, NADW weakens (Henry et al., 2016) and Subantarctic productivity
238 decreases (Anderson et al., 2014; Gottschalk et al., 2016) tracking dust delivery to Antarctica (Fischer
239 et al., 2007) (Figure 4 e, h-i). Ventilation of the SO (as inferred from radiocarbon) improves
240 (Gottschalk et al., 2016; Skinner et al., 2010) and SO upwelling (as inferred from Antarctic
241 productivity) increases (Anderson et al., 2009), although these changes could be more pronounced in
242 the later part of the Heinrich stadials (Figure 4 f-g). During MIS3 all of these changes are largely
243 symmetric around, and consistent with, the minimum in δ¹³C-CO₂ and thus plausible drivers the
244 change in CO₂.

245
246 During the deglaciation some variables trend back towards LGM values after HS1 (NADW and SO
247 upwelling), while others, show near permanent shifts to interglacial levels during HS1 (Subantarctic
248 productivity, SO ventilation). This decoupling allows us to partially disentangle which processes
249 control atmospheric CO₂. Based on relationship between the proxies and atmospheric data in MIS3,
250 we would expect that if changes in NADW and/or SO upwelling were to control atmospheric CO₂, we
251 would observe a large CO₂ decrease and δ¹³C-CO₂ increase in the BA. This is clearly not the case and
252 requires either a muted response to these forcings or another source of carbon in the BA that
253 compensated for the apparent carbon sink. Conversely, if changes in Subantarctic productivity and SO
254 ventilation dominated the atmospheric CO₂ budget, we could expect CO₂ to remain elevated during the
255 BA and δ¹³C-CO₂ to plateau at lower values, a scenario that is in much better agreement with the data.
256 Thus Subantarctic productivity and SO ventilation appear to have a more consistent link with

257 atmospheric CO₂ in both MIS3 and the Last Deglaciation and are strong candidates for contributing
258 significantly to glacial-interglacial CO₂ change.

259

260 **Discussion: Centennial-scale carbon cycle variability**

261 On the centennial-scale our new observations in MIS3 can be combined with recently identified
262 variability in Last Deglaciation to suggest a ubiquitous and consistent coupling of the carbon cycle with
263 abrupt climate change events. In Figure 4j-q we plot variability in greenhouse gases for two categories
264 of centennial-scale events: the onset of interstadials (D08, the Bølling-Allerød and the pre-Boreal) and
265 mid-Heinrich Stadials events (H4 and H1). The changes are plotted as anomalies and the timing is set
266 relative to the mid-point of the rise in CH₄. Note that the Taylor Glacier chronology is synchronized
267 with the WAIS Divide record via CH₄ and thus the phasing of the two ice cores cannot be interpreted.

268

269 The rapid 8 ppm CO₂ rise during HS4 at 39.5 ka likely shares a common origin with a similar event
270 during the deglaciation with HS1 at 16.3 ka (Marcott et al., 2014) (Figure 4l). Both events are
271 associated with carbon isotope minima (Figure 4m). It has been suggested that these mid-stadial
272 events can be tied to the timing of the Heinrich Events and may represent a rapid release of terrestrial
273 carbon to the atmosphere driven by a cooling and drying of the Northern Hemisphere (Bauska et al.,
274 2016). The event in HS4 is consistent with a terrestrial origin as it coincides with an increase in CH₄
275 (Rhodes et al., 2015) (Figure 4j), which may indicate enhanced precipitation of the Southern
276 Hemisphere tropics, and an increase in $\Delta\epsilon_{\text{LAND}}$, which suggests decreased precipitation in the Northern
277 Hemisphere (Seltzer et al., 2017; Severinghaus et al., 2009) (Figure 1h). Constant N₂O indicates either
278 that changes in terrestrial soil temperatures may have been small on the global scale, thus suggesting
279 that precipitation was the dominant driver of the terrestrial carbon loss, or that oxygen-minimum
280 zones in intermediate ocean were relatively stable, possibly indicating the absence of a change ocean
281 circulation across this event (Figure 4k).

282

283 The 6 ppm CO₂ rise at the onset of D08 shares common features with the onset of the BA and
284 Preboreal (~11.5ka) during the deglaciation (Figure 4p). All three events exhibit simultaneous
285 increases in CO₂, CH₄ and N₂O that coincide with abrupt Northern Hemisphere warmings, continued
286 warming or at least stable temperatures in Antarctica (WAIS Divide Project Members, 2015), and
287 greater NADW formation (Henry et al., 2016; McManus et al., 2004) (Figure 3, vertical yellow dashed
288 lines). The $\delta^{13}\text{C-CO}_2$ across all events is variable but shows no secular trend (Preboreal) or slight
289 increase of ~0.08‰ (B/A and D08) (Figure 4q). At face value, this pattern of increasing CO₂ and
290 increasing $\delta^{13}\text{C-CO}_2$ indicates that rising ocean temperature contributed to the CO₂ rise with additional
291 (but limited) changes in the net flux of organic carbon. This simplest of scenarios is somewhat
292 surprising given that changes in the ocean's biological pump may accompany the large and abrupt
293 reorganization of ocean circulation and changes in terrestrial carbon reservoirs are clearly indicated by

294 the large increases in CH₄ and N₂O (Figure 5e). More plausibly, yet more challenging to accurately
295 model, are a roughly synchronous changes in several sources. Recently, the LOVECLIM model, which
296 predicts a small positive relationship between CO₂ and δ¹³C-CO₂ during reduced NADW (Menviel et al.,
297 2015), also predicts increases in CO₂ of 10 to 15 ppm upon the resumption of NADW (with the effect of
298 solubility contributing about 50% to CO₂ variability) (Menviel et al., 2015). Moreover, a precisely
299 dated coral record shows that these events during the last deglaciation are associated with brief
300 intervals of enhanced overturning in the Atlantic (Chen et al., 2015). This integrated response to the
301 onset of an interstadial is consistent with the CO₂ and δ¹³C-CO₂ data, and may be a pervasive feature of
302 last glacial period CO₂ variability, but requires ground-truthing with additional, high-resolution MIS3
303 marine records.

304

305 **Conclusions**

306 Carbon isotope data from the last deglaciation and last glacial period clearly show that CO₂ variability
307 is the sum of multiple mechanisms, many of which are triggered by abrupt climate change. During both
308 periods millennial-scale variability is present and likely associated with the release of respired organic
309 carbon from the deep ocean. Superimposed on these oscillations are two types of centennial-scale
310 changes i) CO₂ increases and δ¹³C-CO₂ decreases in the middle of Heinrich stadials and ii) CO₂
311 increases and small changes in δ¹³C-CO₂ that are in-phase with rapid increases in NH temperature.
312 During the deglaciation the millennial-scale component is enhanced and an additional carbon source is
313 required to sustain the CO₂ rise through the entire deglaciation. This suggests that although abrupt
314 climate variability is not the sole driver of the deglacial CO₂ rise, it may be a prerequisite. These
315 potential links can now be tested with model experiments that use the MIS3 data to constrain the
316 sensitivity to centennial and millennial-scale components and the deglacial data to evaluate how these
317 mechanisms interact with changes in insolation, ice volume and global temperatures.

318

319 **Acknowledgements**

320 This work was funded by NSF grants ANT 0838936 (Oregon State University), ANT 0839031 (Scripps
321 Institution of Oceanography). Data will be made available online at National Climate Data Center:
322 <https://www.ncdc.noaa.gov/paleo/study/24170>

323

324

325

326 **References**

- 327 Ahn, J., & Brook, E. J. (2008). Atmospheric CO₂ and climate on millennial time scales during the last
328 glacial period. *Science*, 322(5898), 83–85. <https://doi.org/10.1126/science.1160832>
- 329 Ahn, J., & Brook, E. J. (2014). Siple Dome ice reveals two modes of millennial CO₂ change during the last
330 ice age. *Nature Communications*, 5, 3723.
- 331 Anderson, R. F., Ali, S., Bradtmiller, L. I., Nielsen, S. H. H., Fleisher, M. Q., Anderson, B. E., & Burckle, L. H.
332 (2009). Wind-Driven Upwelling in the Southern Ocean and the Deglacial Rise in Atmospheric
333 CO₂. *Science*, 323(5920), 1443–1448. <https://doi.org/10.1126/science.1167441>
- 334 Anderson, R. F., Barker, S., Fleisher, M., Gersonde, R., Goldstein, S. L., Kuhn, G., et al. (2014). Biological
335 response to millennial variability of dust and nutrient supply in the Subantarctic South Atlantic
336 Ocean. *Philosophical Transactions of the Royal Society of London A: Mathematical, Physical and*
337 *Engineering Sciences*, 372(2019). <https://doi.org/10.1098/rsta.2013.0054>
- 338 Baggenstos, D., Bauska, T. K., Severinghaus, J. P., Lee, J. E., Schaefer, H., Buizert, C., et al. (2017).
339 Atmospheric gas records from Taylor Glacier, Antarctica, reveal ancient ice with ages spanning
340 the entire last glacial cycle. *Climate of the Past*, 13(7), 943–958. [https://doi.org/10.5194/cp-](https://doi.org/10.5194/cp-13-943-2017)
341 [13-943-2017](https://doi.org/10.5194/cp-13-943-2017)
- 342 Barker, S., & Diz, P. (2014). Timing of the descent into the last Ice Age determined by the bipolar
343 seesaw. *Paleoceanography*, 29(6), 489–507. <https://doi.org/10.1002/2014PA002623>
- 344 Bauska, T. K., Brook, E. J., Mix, A. C., & Ross, A. (2014). High-precision dual-inlet IRMS measurements of
345 the stable isotopes of CO₂ and the N₂O / CO₂ ratio from polar ice core samples. *Atmos. Meas.*
346 *Tech.*, 7(11), 3825–3837. <https://doi.org/10.5194/amt-7-3825-2014>
- 347 Bauska, T. K., Joos, F., Mix, A. C., Roth, R., Ahn, J., & Brook, E. J. (2015). Links between atmospheric
348 carbon dioxide, the land carbon reservoir and climate over the past millennium. *Nature*
349 *Geoscience*, 8, 383–387. <https://doi.org/10.1038/ngeo2422>
- 350 Bauska, T. K., Baggenstos, D., Brook, E. J., Mix, A. C., Marcott, S. A., Petrenko, V. V., et al. (2016). Carbon
351 isotopes characterize rapid changes in atmospheric carbon dioxide during the last
352 deglaciation. *Proceedings of the National Academy of Sciences*, 113(13), 3465–3470.
353 <https://doi.org/10.1073/pnas.1513868113>

- 354 Bereiter, B., Lüthi, D., Siegrist, M., Schüpbach, S., Stocker, T. F., & Fischer, H. (2012). Mode change of
355 millennial CO₂ variability during the last glacial cycle associated with a bipolar marine carbon
356 seesaw. *Proceedings of the National Academy of Sciences*, 109(25), 9755–9760.
357 <https://doi.org/10.1073/pnas.1204069109>
- 358 Broecker, W. S., & McGee, D. (2013). The ¹³C record for atmospheric CO₂: What is it trying to tell us?
359 *Earth and Planetary Science Letters*, 368(0), 175–182.
360 <https://doi.org/10.1016/j.epsl.2013.02.029>
- 361 Brook, E. J., Harder, S., Severinghaus, J., Steig, E. J., & Sucher, C. M. (2000). On the origin and timing of
362 rapid changes in atmospheric methane during the last glacial period. *Global Biogeochemical*
363 *Cycles*, 14(2), 559–572.
- 364 Buizert, C., Cuffey, K. M., Severinghaus, J. P., Baggenstos, D., Fudge, T. J., Steig, E. J., et al. (2015). The
365 WAIS Divide deep ice core WD2014 chronology – Part 1: Methane synchronization (68–31 ka
366 BP) and the gas age–ice age difference. *Clim. Past*, 11(2), 153–173.
367 <https://doi.org/10.5194/cp-11-153-2015>
- 368 Charles, C. D., Lynch-Stieglitz, J., Ninnemann, U. S., & Fairbanks, R. G. (1996). Climate connections
369 between the hemisphere revealed by deep sea sediment core/ice core correlations. *Earth and*
370 *Planetary Science Letters*, 142(1), 19–27. [https://doi.org/10.1016/0012-821X\(96\)00083-0](https://doi.org/10.1016/0012-821X(96)00083-0)
- 371 Charles, C. D., Pahnke, K., Zahn, R., Mortyn, P. G., Ninnemann, U., & Hodell, D. A. (2010). Millennial scale
372 evolution of the Southern Ocean chemical divide. *Quaternary Science Reviews*, 29(3–4), 399–
373 409. <http://dx.doi.org/10.1016/j.quascirev.2009.09.021>
- 374 Chen, T., Robinson, L. F., Burke, A., Southon, J., Spooner, P., Morris, P. J., & Ng, H. C. (2015). Synchronous
375 centennial abrupt events in the ocean and atmosphere during the last deglaciation. *Science*,
376 349(6255), 1537–1541. <https://doi.org/10.1126/science.aac6159>
- 377 Cheng, H., Edwards, R. L., Sinha, A., Spötl, C., Yi, L., Chen, S., et al. (2016). The Asian monsoon over the
378 past 640,000 years and ice age terminations. *Nature*, 534, 640.
- 379 Clark, P. U., Shakun, J. D., Marcott, S. A., Mix, A. C., Eby, M., Kulp, S., et al. (2016). Consequences of
380 twenty-first-century policy for multi-millennial climate and sea-level change. *Nature Clim.*
381 *Change*, 6(4), 360–369.

382 Eggleston, S., Schmitt, J., Bereiter, B., Schneider, R., & Fischer, H. (2016). Evolution of the stable carbon
383 isotope composition of atmospheric CO₂ over the last glacial cycle. *Paleoceanography*, 31(3),
384 434–452. <https://doi.org/10.1002/2015PA002874>

385 Ehleringer, J. R., Cerling, T. E., & Helliker, B. R. (1997). C₄ photosynthesis, atmospheric CO₂, and
386 climate. *Oecologia*, 112(3), 285–299. <https://doi.org/10.1007/s004420050311>

387 Fischer, H., Fundel, F., Ruth, U., Twarloh, B., Wegner, A., Udisti, R., et al. (2007). Reconstruction of
388 millennial changes in dust emission, transport and regional sea ice coverage using the deep
389 {EPICA} ice cores from the Atlantic and Indian Ocean sector of Antarctica. *Earth and Planetary
390 Science Letters*, 260(1–2), 340–354. <http://dx.doi.org/10.1016/j.epsl.2007.06.014>

391 Gottschalk, J., Skinner, L. C., Lippold, J., Vogel, H., Frank, N., Jaccard, S. L., & Waelbroeck, C. (2016).
392 Biological and physical controls in the Southern Ocean on past millennial-scale atmospheric
393 CO₂ changes. *Nature Communications*, 7, 11539.

394 Henry, L. G., McManus, J. F., Curry, W. B., Roberts, N. L., Piotrowski, A. M., & Keigwin, L. D. (2016). North
395 Atlantic ocean circulation and abrupt climate change during the last glaciation. *Science*,
396 353(6298), 470–474. <https://doi.org/10.1126/science.aaf5529>

397 Hodell, D. A., Kanfoush, S. L., Shemesh, A., Crosta, X., Charles, C. D., & Guilderson, T. P. (2001). Abrupt
398 cooling of Antarctic surface waters and sea ice expansion in the South Atlantic sector of the
399 Southern Ocean at 5000 cal yr B.P. *Quaternary Research*, 56(2), 191–198.

400 Hodell, D. A., Venz, K. A., Charles, C. D., & Ninnemann, U. S. (2003). Pleistocene vertical carbon isotope
401 and carbonate gradients in the South Atlantic sector of the Southern Ocean. *Geochemistry
402 Geophysics Geosystems*, 4. <https://doi.org/10.1029/2002gc000367>

403 Indermuhle, A., Wahlen, M. .. Monnin, E. .. Stauffer, B. .. Stocker, T. F. (2000). Atmospheric CO₂
404 concentration from 60 to 20 kyr BP from the Taylor Dome ice core, Antarctica. *Geophysical
405 Research Letters*, 27(5), 735–738.

406 Jaccard, S. L., Galbraith, E. D., Martínez-García, A., & Anderson, R. F. (2016). Covariation of deep
407 Southern Ocean oxygenation and atmospheric CO₂ through the last ice age. *Nature*, 530, 207–
408 210.

409 Kohler, P., Fischer, H., Schmitt, J., & Munhoven, G. (2006). On the application and interpretation of
410 Keeling plots in paleo climate research - deciphering delta C-13 of atmospheric CO₂ measured
411 in ice cores. *Biogeosciences*, 3(4), 539–556.

412 Marcott, S. A., Bauska, T. K., Buizert, C., Steig, E. J., Rosen, J. L., Cuffey, K. M., et al. (2014). Centennial-
413 scale changes in the global carbon cycle during the last deglaciation. *Nature*, 514(7524), 616–
414 619.

415 Martínez-García, A., Sigman, D. M., Ren, H., Anderson, R. F., Straub, M., Hodell, D. A., et al. (2014). Iron
416 Fertilization of the Subantarctic Ocean During the Last Ice Age. *Science*, 343(6177), 1347.
417 <https://doi.org/10.1126/science.1246848>

418 McManus, J. F., Francois, R., Gherardi, J. M., Keigwin, L. D., & Brown-Leger, S. (2004). Collapse and rapid
419 resumption of Atlantic meridional circulation linked to deglacial climate changes. *Nature*,
420 428(6985), 834–837. <https://doi.org/10.1038/nature02494>

421 Menviel, L., Joos, F., & Ritz, S. P. (2012). Simulating atmospheric CO₂, ¹³C and the marine carbon cycle
422 during the Last Glacial–Interglacial cycle: possible role for a deepening of the mean
423 remineralization depth and an increase in the oceanic nutrient inventory. *Quaternary Science*
424 *Reviews*, 56, 46–68.

425 Menviel, L., Spence, P., & England, M. H. (2015). Contribution of enhanced Antarctic Bottom Water
426 formation to Antarctic warm events and millennial-scale atmospheric {CO₂} increase. *Earth*
427 *and Planetary Science Letters*, 413, 37–50. <http://dx.doi.org/10.1016/j.epsl.2014.12.050>

428 Menviel, Laurie, Mouchet, A., Meissner, K., Joos, F., & England, M. (2015). Impact of oceanic circulation
429 changes on atmospheric δ¹³CO₂. *Global Biogeochemical Cycles*, 29(11), 1944–1961.

430 North Greenland Ice Core Project Members. (2004). High-resolution record of Northern Hemisphere
431 climate extending into the last interglacial period. *Nature*, 431(7005), 147–151.

432 Ninnemann, U. S., Charles, C. D., & Hodell, D. A. (1999). Origin of Global Millennial Scale Climate Events:
433 Constraints from the Southern Ocean Deep Sea Sedimentary Record. In *Mechanisms of Global*
434 *Climate Change at Millennial Time Scales* (pp. 99–112). American Geophysical Union.
435 <https://doi.org/10.1029/GM112p0099>

436 Rhodes, R. H., Brook, E. J., Chiang, J. C. H., Blunier, T., Maselli, O. J., McConnell, J. R., et al. (2015).
437 Enhanced tropical methane production in response to iceberg discharge in the North Atlantic.
438 *Science*, 348(6238), 1016–1019. <https://doi.org/10.1126/science.1262005>

439 Schilt, A., Baumgartner, M., Schwander, J., Buiron, D., Capron, E., Chappellaz, J., et al. (2010).
440 Atmospheric nitrous oxide during the last 140,000 years. *Earth and Planetary Science Letters*,
441 300(1–2), 33–43. <https://doi.org/10.1016/j.epsl.2010.09.027>

442 Schilt, Adrian, Brook, E. J., Bauska, T. K., Baggenstos, D., Fischer, H., Joos, F., et al. (2014). Isotopic
443 constraints on marine and terrestrial N₂O emissions during the last deglaciation. *Nature*,
444 516(7530), 234–237.

445 Schmitt, J., Schneider, R., Elsig, J., Leuenberger, D., Lourantou, A., Chappellaz, J., et al. (2012). Carbon
446 Isotope Constraints on the Deglacial CO₂ Rise from Ice Cores. *Science*, 336(6082), 711–714.
447 <https://doi.org/10.1126/science.1217161>

448 Schmittner, A., & Lund, D. C. (2015). Early deglacial Atlantic overturning decline and its role in
449 atmospheric CO₂ rise inferred from carbon isotopes ($\delta^{13}\text{C}$). *Clim. Past*, 11(2), 135–152.
450 <https://doi.org/10.5194/cp-11-135-2015>

451 Seltzer, A. M., Buizert, C., Baggenstos, D., Brook, E. J., Ahn, J., Yang, J.-W., & Severinghaus, J. P. (2017).
452 Does $\delta^{18}\text{O}$ of O₂ record meridional shifts in tropical rainfall? *Climate of the Past*, 13(10), 1323–
453 1338. <https://doi.org/10.5194/cp-13-1323-2017>

454 Severinghaus, J. P., Beaudette, R., Headly, M. A., Taylor, K., & Brook, E. J. (2009). Oxygen-18 of O₂
455 Records the Impact of Abrupt Climate Change on the Terrestrial Biosphere. *Science*, 324(5933),
456 1431–1434. <https://doi.org/10.1126/science.1169473>

457 Sigman, D. M., Hain, M. P., & Haug, G. H. (2010). The polar ocean and glacial cycles in atmospheric CO₂
458 concentration. *Nature*, 466(7302), 47–55. <https://doi.org/10.1038/nature09149>

459 Skinner, L. C., Fallon, S., Waelbroeck, C., Michel, E., & Barker, S. (2010). Ventilation of the Deep
460 Southern Ocean and Deglacial CO₂ Rise. *Science*, 328(5982), 1147–1151.
461 <https://doi.org/10.1126/science.1183627>

462 Tschumi, T., Joos, F., Gehlen, M., & Heinze, C. (2011). Deep ocean ventilation, carbon isotopes, marine
463 sedimentation and the deglacial CO₂ rise. *Climate of the Past*, 7(3), 771–800.
464 <https://doi.org/10.5194/cp-7-771-2011>

465 WAIS Divide Project Members. (2015). Precise inter-polar phasing of abrupt climate change during the
466 last ice age. *Nature*, 520(7549), 661–665.

467 Ziegler, M., Diz, P., Hall, I. R., & Zahn, R. (2013). Millennial-scale changes in atmospheric CO₂ levels
468 linked to the Southern Ocean carbon isotope gradient and dust flux. *Nature Geosci*, 6(6), 457–
469 461.

470

471 **Figure 1**
472 Taylor Glacier CO₂, CH₄, N₂O and δ¹³C-CO₂ (blue markers with black smoothing spline, *this study*).
473 Panel A: NGRIP δ¹⁸O(North Greenland Ice Core Project Members, 2004). B: WDC δ¹⁸O(WAIS Divide
474 Project Members, 2015). C: Hulu Cave δ¹⁸O (Cheng et al., 2016) D: WDC (Rhodes et al., 2015) (thin
475 black line) and Taylor Glacier CH₄. E: Siple Dome (Ahn & Brook, 2014)(gray markers) and Taylor
476 Glacier CO₂. F: Taylor Glacier δ¹³C-CO₂. G: Talos Dome (Schilt et al., 2010) (gray markers) and Taylor
477 Glacier N₂O. H: Global Terrestrial O₂ isotopic fractionation, Δ_{ELAND}, constrained from a combination of
478 WDC and Siple Dome (Seltzer et al., 2017; Severinghaus et al., 2009). Dotted lines highlight the stadial
479 to interstadial transitions and the red bar highlights the Heinrich Stadial with the associated rise in
480 CO₂, CH₄ and increase in Δ_{ELAND}. The NGRIP chronology is increased by 0.63% prior to 22ka for
481 consistency with the WDC chronology (WAIS Divide Project Members, 2015).

482
483 **Figure 2**
484 Cross-plot of atmospheric CO₂ and δ¹³C-CO₂ spanning the MIS3 section (blue, *this study*) and the last
485 deglaciation, which is subdivide into the LGM to HS1 data (red) and late-Deglaciation (gray). Solid
486 lines indicate linear regressions through the MIS3 (blue) and HS1 (red) data.

487
488 **Figure 3**
489 Comparison of atmospheric record of δ¹³C-CO₂ with oceanic records of δ¹³C and nutrient utilization. A:
490 Atmospheric δ¹³C-CO₂ (*this study*) on an inverted y-axis. B: The difference in δ¹³C between Sub-
491 Antarctic mode water (SAMW) and circumpolar deepwater (CDW)(Ziegler et al., 2013). A stack of
492 benthic δ¹³C (black line) from a combination of record in the deep Southern Ocean (grey circles)
493 (Charles et al., 1996; Hodell et al., 2001, 2003; Ninnemann et al., 1999). Also indicated is the
494 uncertainty on these chronologies (Barker & Diz 2014) based on synchronization between carbonate
495 preservation and Greenland temperature (black boxes) and independent age control based on the
496 Laschamp event (blue boxes). D: Foraminifera-bound δ¹⁵N indicating nitrate consumption in
497 Subantarctic (Martínez-García et al., 2014). Red bars highlight the broad millennia-scale correlations.

499
500 **Figure 4**
501 Left Panel: Comparison of MIS3 data (*this study*) and Last Deglaciation (Bauska et al., 2016; Marcott et
502 al., 2014; Rhodes et al., 2015) greenhouse gas variability. A: WDC CH₄ (Rhodes et al., 2015). B: Taylor
503 Glacier N₂O. C: Taylor Glacier CO₂. D: Taylor Glacier δ¹³C-CO₂. E: Pa/Th, a proxy for the strength of
504 NADW formation (Henry et al., 2016; McManus et al., 2004)(orange), F: the opal flux in the
505 SO(Anderson et al., 2009), a proxy for upwelling (green) (note the two different cores and axes are
506 used in the comparison), G: the benthic to atmosphere ¹⁴C age reconstructions for the Subantarctic
507 zone(Gottschalk et al., 2016; Skinner et al., 2010), H: nssCa flux from the EDML ice core(Fischer et al.,
508 2007), a proxy for dust delivery to Antarctica (brown), I: opal flux in the Subantarctic zone(Gottschalk

509 et al., 2016), a proxy for productivity (from the same core as the ventilation reconstruction). Yellow
510 bars highlight the onset of interstadial conditions, black bars indicated the initial CO₂ rises and red bars
511 correspond to the rapid jumps in CO₂ and CH₄. Right Panel: Centennial-scale variability during the last
512 glacial period from Taylor Glacier and WAIS Divide. Anomalies in the concentration and isotopic
513 composition of the greenhouse gases are plotted with the relative timing determined by the mid-point
514 in the CH₄ rise. Marker color corresponds to dashed lines in left panel.

515

516

517

518

519

Figure 1.

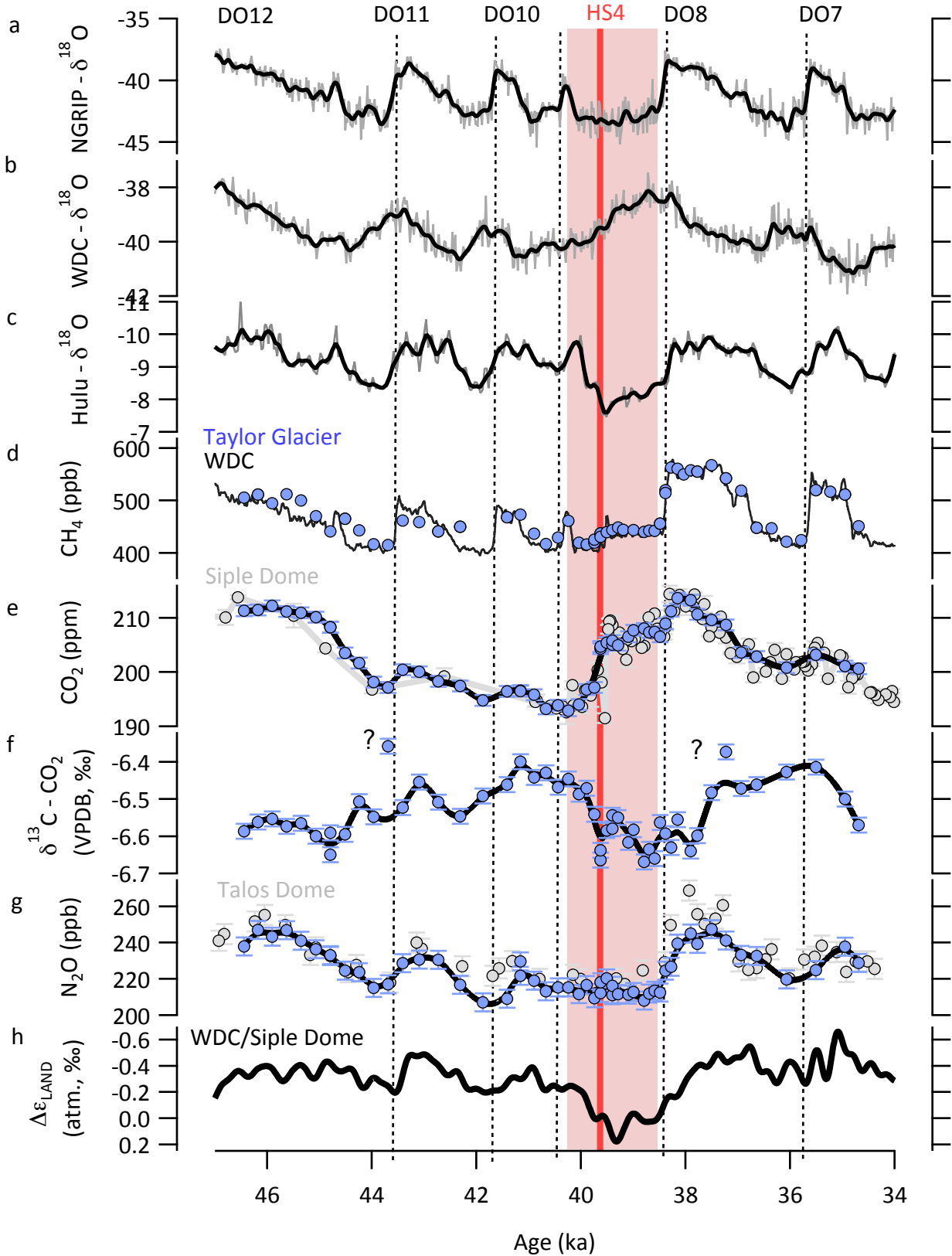


Figure 2.

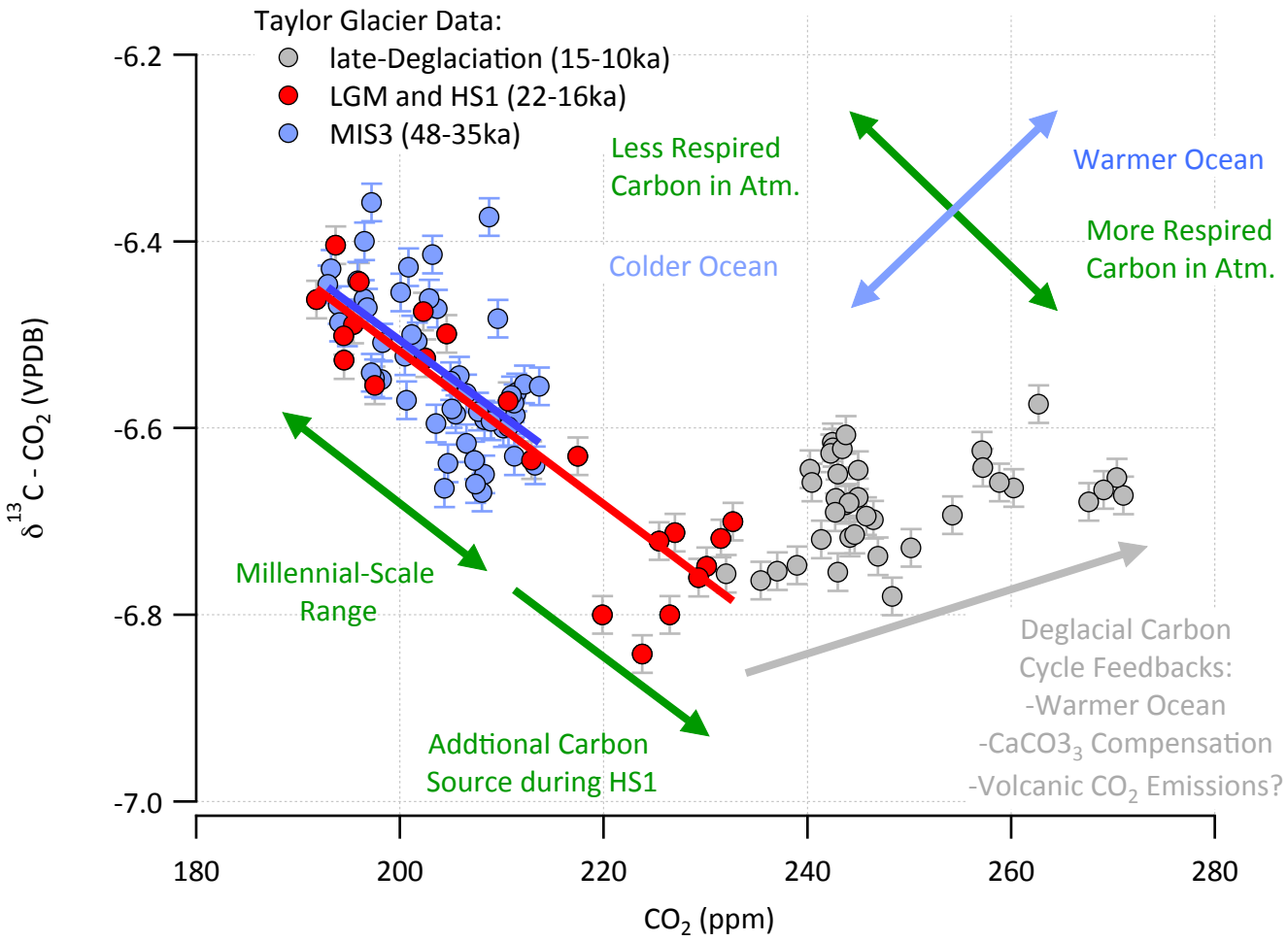


Figure 3.

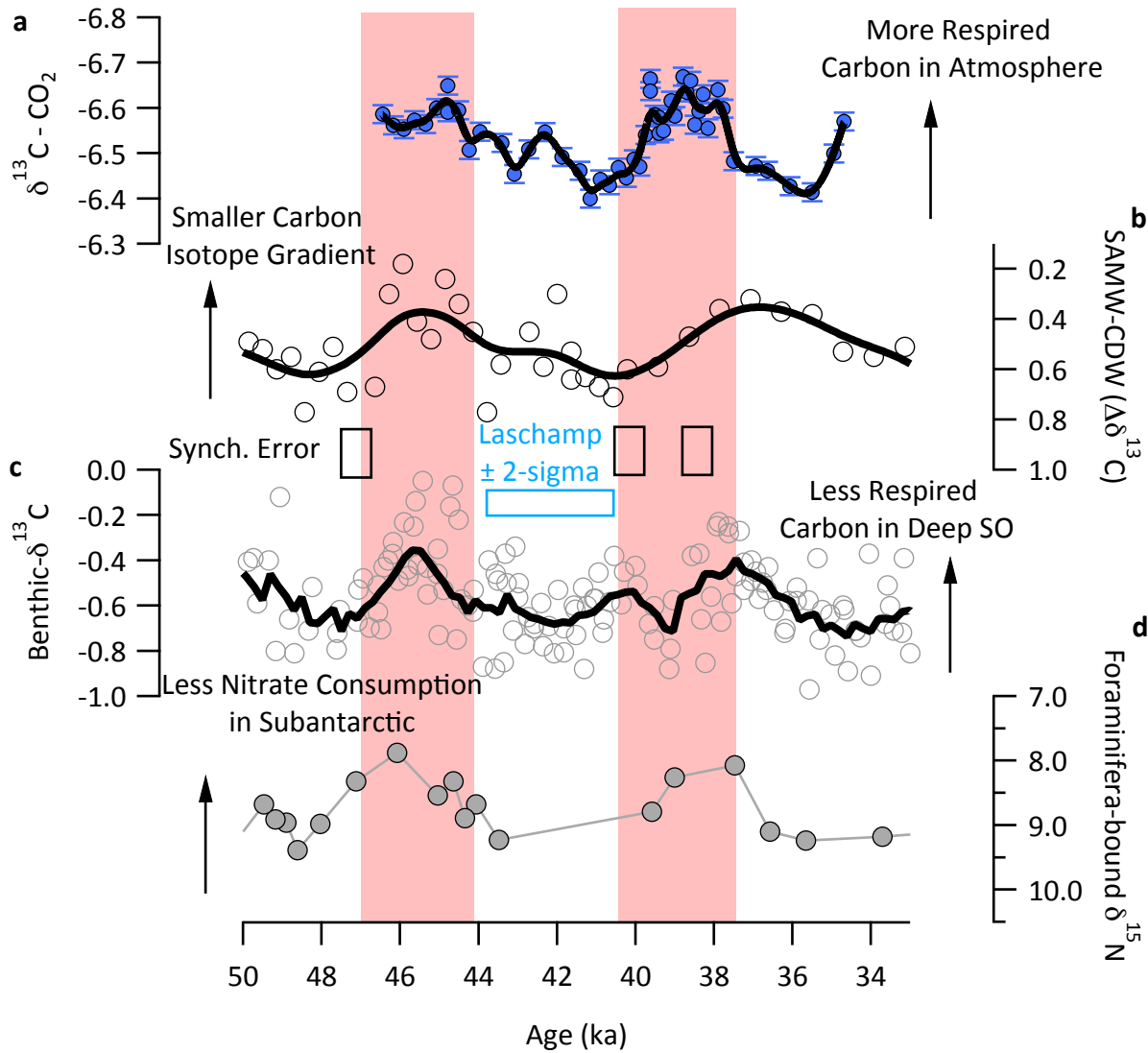


Figure 4.

